SSRG International Journal of Civil Engineering
ISSN: 2348-8352/ https://doi.org/10.14445/23488352/IJCE-V13I3P124

Volume 13 Issue 3, 335-351, March 2026

Original Article

The Flexural Efficiency and Effectiveness of Geometrically Interlocked Layered Wood-Plastic Composite Beams

Eduard Darrel P. Rivera[1], Dexter Hansel C. Apnoyan[1]

[1]*College of Engineering and Architecture, University of the Cordilleras, Baguio City, Philippines.*

[1]*Corresponding Author : standardemman@yahoo.com*

Received: 17 December 2025 Revised: 20 January 2026 Accepted: 25 February 2026 Published: 23 March 2026

Abstract *- The concept of topological and geometrical interlocking is an atypical method of assembling built-up sections and composites. It is commonly demonstrated in traditional woodworking techniques, where components are joined without mechanical fasteners or chemical adhesives. The paper explored its structural application to modern materials and construction practice by examining three two-layered wood-plastic composite beams whose components were solely interlocked by 45-degree grooves or notches. The beams were produced as test specimens and were analyzed for their yielding and rupturing flexural effectiveness and efficiencies. The effectiveness compares their full composite theoretical flexural strengths to their actual values, while the efficiencies determine their capacity to retain full composite action during bending. The theoretical calculations incorporated classical elastic and plastic beam theories, and the actual values were determined by a standard three-point bending test. The analysis showed that the beam specimens achieved, on average, 66.98 percent of their theoretical full composite flexural strength at yield and 55.59 percent at rupture while maintaining an average full composite behavior of 78.53 percent at yield and 59.55 percent at rupture. Results of the experiment described the beam specimens as unable to retain constant efficiency and only able to realize subpar flexural strengths. While the evidence concluded them to be partial composites, the analyzed data showed that the peaks in efficiency and effectiveness generally occurred during yield and then continuously decayed post-yield until rupture.*

Keywords *- Effectiveness, Efficiencies, Full composite, Geometrical, Topological interlocking.*

1. Introduction

At present, the assembly of composite beams and other built-up sections is ordinarily done through fasteners or chemical bonding, such as bolting or gluing components together in layers. While the reliability of these common methods is not questioned, the innovation to explore other means of assemblage is found wanting amid an age where advanced materials, such as plastics, are continuously being studied. The current dominance of ordinary methods in assembling composites and built-up sections may cause the potential of other atypical methods to be left undiscovered in material research.

An alternative atypical method in assembling composites is offered by the concept of topological and geometrical interlocking (TGI). The principle is defined as the mechanical locking of discrete elements in an assemblage through kinematic constraints imposed by its neighboring components through the virtue of element geometry and mutual arrangements of the subunits within the structure or composite [1]. This concept is evident in notable examples of Asian classical and traditional wooden architecture, particularly in Japanese shrines and temples that have survived to the present day. Through generations of expertise, the Japanese craftsmen became exceedingly versed in timber construction and in finding ways to establish a sound system for timber joinery without the use of nails or adhesives. The result of this tradition is a number of wood joining techniques and connecting methods capable of erecting buildings that can even stand in areas of frequent seismic activity [2]. However, the traditional Japanese style of construction is in decline, as reproducing the joineries depends on highly skilled labor that takes roughly 15 years to train [3]. Moreover, the increasing preference in the current construction industry for more sustainable and modern materials, such as steel and concrete, over wood has further reduced its use. Despite these challenges, the study believes the difficulties in reproduction can be alleviated by current and at hand technologies such as power tools. In addition, it is presently convenient that emerging advanced construction materials that are flexible and durable enough to be shaped, especially plastics, exist and apparently offer compatibility with TGI. Collectively, these

considerations justified the examination of applying TGI in the current era.

The paper gauges the flexural performance in applying TGI to three Two Layered Composite Beam (TLCB) assemblies made of wood and plastic by the criteria of flexural effectiveness and efficiency. The flexural effectiveness measures the actual capability of the beams to reach their theoretical full composite flexural strength, while their efficiency quantifies how much of the full composite action is retained during bending. By analyzing these flexural properties in wood-plastic composite beams, the structural viability of using TGI with modern materials can be estimated. The data and results in the study serve as a stepping stone and reference for future researchers attempting the implementation of a similar concept, and help justify the investment and resources to pursue it. Further, the paper spotlights alternatives for assembling composites and encourages the traditional methods in construction to be reviewed and innovated upon for present use.

2. Materials and Methods

2.1. Research Guideline

The paper was conceptualized as being part of an introductory research to applying TGI in assembling structural composite members by examining the bending behaviour of three TLCB specimens. Only two flexural behavior properties at the elastic yield and rupture stages of bending were measured to describe their flexural performance, defined by their flexural effectiveness and efficiency. As much as the paper focuses on these two properties, the raw data and other findings from the experiment, such as deflections, flexural strength, failure modes, theoretical analyses, and observations, were also presented.

All three beam specimens were produced from the same wood and plastic materials and were assembled in the same manner. The components were interlocked through 45-degree grooves that fit into and cut across one another, forming a composite section with the wood layer configured on top and the plastic layer on the bottom. The wood and plastic materials were procured within the research locale. The wood component came from three commercial Russian Pine planks of the same size and supplier, and the plastic component came from a single solid polycarbonate sheet.

The geometric section of the beam specimens was generally dictated by the commercially pre-cut wooden planks, to which the plastic sheet was cut to match their commercial width and length. Ultimately, the plastic sheet was able to supply three TLCB specimens, and the researchers were only able to afford one sheet, where it may have been preferable to produce more specimens to examine. Further, as a prerequisite to the calculations for the theoretical flexural strengths and deformations of the TLCB specimens, it was required that the flexural properties and shear strength parallel to the grain of the components be determined through standard material testing. The samples for these tests were taken from the remaining material volumes of the TLCB specimens, in which they allotted one flexural sample and one shear sample from each of the three wood planks, and four flexural samples from the plastic sheet to be made.

The calculations for the theoretical flexural strengths and deformations of the TLCB specimens incorporated classical elastic and plastic beam theories. Their elastic flexural behavior was solved mainly through the Transformed Section Method, and their post-elastic or plastic behavior was determined by simple plastic theories, which comprise several assumptions that ease these computations. While more sophisticated models and methods exist, such as matrix-based analysis, finite element method, or through computer software, this paper partly serves to aid future researchers in deciding if they should immediately involve these more complex solutions.

The results of the calculations functioned as the baseline for the actual measured flexural strengths and deformations of the TLCB specimens to realize. The comparisons between their respective actual measurements and theoretical calculations at yielding and rupture determined their effectiveness and efficiency at these bending stages. The actual measurements were determined by a three-point bending test with a Universal Testing Machine (UTM). The procedure of the test, including the material tests for the TLCB components, was governed by the standard procedures from the American Society for Testing and Materials (ASTM).

2.2. Composite Behavior

Composite action or behavior describes the interaction between the components of layered composites or built-up assemblies. They are bounded by two extreme limits: the full and non-composite behavior. Full composite behavior is the upper limit wherein the interface between the components is considered perfectly bonded and allows no relative motion or slip. Non-composite behavior defines the lower limit, which considers the components being completely unbounded, without friction, and allows no interaction between them to take place.

Realistically, actual systems are stiffer than when they theoretically act as a non-composite while being less stiff than when they are considered as a full composite [4]. Moreover, full composite behavior implies that the composite beam components act in unison and therefore share a singular bending neutral axis; any less would create separate neutral axes for each component. On the opposite side of this behavior, the axes for non-composites would initially be located at each of the components' geometric centers. It should be noted that the stress profile of the whole beam section is in equilibrium regardless of the number of bending neutral axes. Otherwise, these axes will shift, especially when plastic behavior is involved.

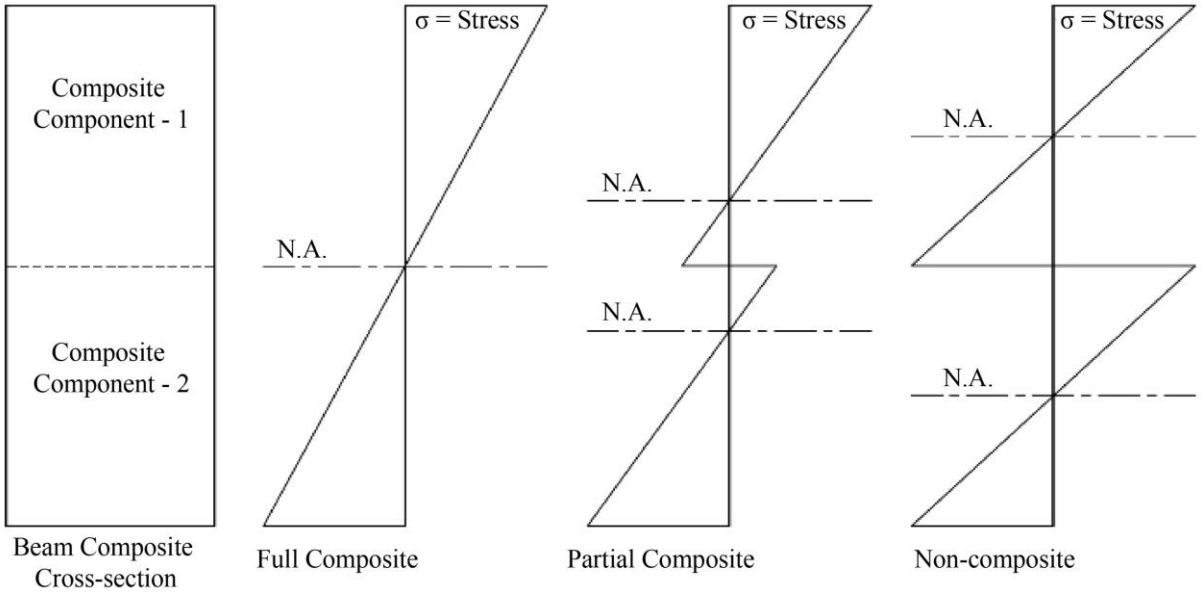

Fig. 1 Typical composite beam stress profiles for different composite behaviors

2.3. Flexural Effectiveness and Efficiency

In this paper, the flexural effectiveness and efficiencies of the TLCB specimens were evaluated at the yielding and rupturing stages of bending since the developed stress and strain relationship during yield and post-yield are different for all materials, in reference to elastic and plastic behavior. These properties were determined through the verification of theoretical predictions with experimental results using the functions presented in Equations 1 and 2. While variations between the two stages were anticipated, the general equations used to determine these properties remained the same.

The effectiveness of the beam specimens was calculated by dividing their actual yielding or rupturing moment by their respective full composite theoretical flexural strength.

$$EFV = \left(\frac{M_{Abm}}{M_{Tbm}}\right) 100\% \quad (1)$$

Where *EFV* is the effectiveness of the TLCB specimen, M_{Abm} is the actual moment on the beam during yield or rupture, and M_{Tbm} is the corresponding full composite theoretical moment capacity.

The efficiency of the composite beams is found through their theoretical and actual deformations during actual yield and rupture. They are computed by dividing the difference between the theoretical non-composite and actual deformations by the difference between the non-composite and full composite theoretical deformations [5]. The theoretical full and non-composite deformations are treated as the baselines for the actual deformations to realize.

$$EFF = \left(\frac{\Delta_N - \Delta_I}{\Delta_N - \Delta_C}\right) 100\% \quad (2)$$

Where, *EFF* is the efficiency of the TLCB specimen, Δ_N is the theoretical deformation of the assumed non-composite beam, Δ_I is the measured actual deformation of the beam, and Δ_C is the theoretical deformation of the full composite beam.

2.4. Composite Beam Properties

2.4.1. Specimen Production

The three TLCB specimens were produced using a combination of hand and power tools, including power saws, routers, drills, sanders, and files. Their components were intentionally shaped to the dimensions shown in Figure 2. Each specimen consisted of a commercial Russian Pine wood top layer and a solid polycarbonate bottom layer. The wood layers for each specimen were sourced from separate planks, while the plastic layers were taken from a single sheet. The cut and fit in 45-degree and 5.85mm deep groves served to join the components together, ideally preventing them from separation during bending.

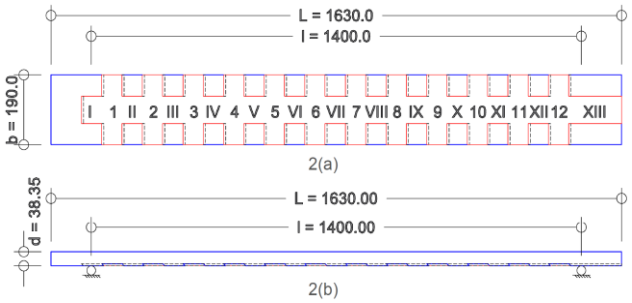

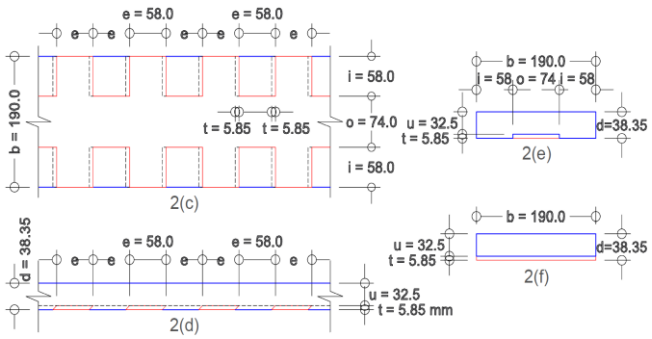

Fig. 2(a) Typical Composite Beam Top Dimensions, (b) Typical Composite Beam Profile Dimensions, (c) Typical Composite Beam Bottom Blow-up Dimensions, (d) Typical Composite Beam Side Blow-up Dimensions, (e) Typical Beam Sections at I-XIII, and (f) Typical Beam Sections at 1-12.

During the procurement of the components, it was found that retaining the commercial thickness of both components and the commercial width of the wood planks was more practical for the study since they only caused maximum variations of +2.0mm to the total width and +0.97mm to the total depth from the intended dimension of the TLCB specimens. This left the grooves and length of both components and the width of the plastic component to be manually cut and shaped. Even with these technological advantages, minor discrepancies between the resulting dimensions and the intended measurements were found. While no variations were seen on the total length and groove depths of the TLCB specimens, they were present on their groove widths. Maximum variations of 0.95mm, 0.95mm, and 1.10mm averaged at 0.40mm, 0.04mm, and 0.71mm on groove widths "e" and maximum variations of 0.60mm, 0.50mm, and 0.50mm averaged at 0.20mm, 0.40mm, and 0.10mm on groove widths "i" for Samples 1, 2 and 3 respectively were observed. These variations caused adjacent dimensions to adjust as summarized in Table 1. These adjustments were considered minor in the study since, after the assembly of the TLCB specimens, they neither fell apart nor showed apparent signs of the components separating.

Fig. 3(a) Bottom side of composite beam specimens, and (b) Top side of composite beam specimens.

Table 1. Composite beam specimen actual dimensions

Composite Beam Sample Designation	Total Length L, (mm)	Total Depth d, (mm)	Total Width b, (mm)	Plastic Thickness t, (mm)	Wood Thickness u, (mm)	Average Wood Groove Width e_{ave}, (mm)
Sample-1	1630.0	39.22	191.0	5.85	33.37	58.40
Sample-2	1630.0	39.32	192.0	5.85	33.47	58.04
Sample-3	1630.0	38.62	191.0	5.85	32.77	58.71
Target Dimensions	1630.0	38.35	190.0	5.85	32.50	58.00
Composite Beam Sample Designation	Wood Groove Width at Midspan e_m, (mm)	Midspan Wood Dim. i_m, (mm)	Average Wood Dim. i_{ave}, (mm)	Midspan Wood & Plastic Dimension o_m, (mm)	Average Wood & Plastic Dimension o_{ave}, (mm)	Average Spacing of Wood Grooves at Midspan s_{mave}, (mm)
Sample-1	58.60	58.6	58.2	73.8	74.6	116.95
Sample-2	57.70	58.6	58.4	74.9	75.1	116.54
Sample-3	58.90	58.3	58.1	74.4	74.7	116.77
Target Dimensions	58.00	58.0	58.0	74.0	74.0	116.00

2.4.2. Component Mechanical Properties

The calculations for the theoretical flexural strengths and deformations were dependent on the flexural material properties of the components, such as their flexural compressive and tensile strengths, Modulus Of Elasticity (MOE), and shear strength. These properties were determined through standard testing by ASTM D143: Standard Test Methods for Small Clear Specimens of Timber [6] for the wood component and ASTM D790: Standard Test Methods for Flexural Properties of Unreinforced and Reinforced Plastics and Electrical Insulating Materials [7] for the plastic component.

The number of samples used for the tests was controlled by the available suitable material left after the assembly of TLCB specimens, while it would have been more favourable, by the standards, to test more samples.

One flexural sample from each of the three wood planks for the TLCB specimens was taken and subjected to the three-point bending test as prescribed by ASTM D143. These samples represented the properties of each respective plank and not all of the wood components collectively, since each of them may have had different storage conditions or unapparent imperfections during their procurement. Each sample was sized exactly 410mm in length and approximately 25mm in width, and 25mm in depth.

Two roller supports were equally placed 360mm along their length and loaded with a concentrated load at the middle span with a rate of 1.3mm/min by a UTM until rupture. The forces and flexural stress profiles with the displacements and strains were noted throughout the tests. Critical conditions were identified at the proportional limit, elastic limit, and rupture, which determined their flexural compressive and tensile strengths.

Table 2. Wood component flexural strength

Wood Component Beam Sample Designation	Proportional Limit Stress or Comp. Yield Strength (MPa)	Elastic Limit Stress or Tensile Yield Strength (MPa)	Rupture Stress or Tensile Ultimate Strength (MPa)
Sample-1	23.08	34.54	38.82
Sample-2	41.76	64.97	67.97
Sample-3	21.33	31.48	34.59

The same number of samples from the same sources was used for the shear test. Each sample was cut into rectangular prisms with approximate dimensions of 63mm in height, 50mm in width, and 50mm in thickness. A notch of 13mm height, 20mm width, and 50mm thick was cut into the corner of each sample that served to receive the testing shear load parallel to the wood grain. The shear test procedure from ASTM D143 affixed the samples from movement while loading them with a compressive load on the notches, thus applying shear.

The load was applied at a rate of 0.6mm/min from a UTM until rupture, and the developed shear stresses were recorded. The shear strength parallel to the grain of the wood component for TLCB Samples 1, 2, and 3 was found to be 2.71MPa, 8.59MPa, and 10.31MPa, respectively.

The flexural testing procedure for plastic samples outlined in ASTM D790 is similar to that in ASTM D143; however, the test specimens are smaller. Four plastic flexural samples were cut from the same solid polycarbonate sheet supplying the plastic layers for the TLCB specimens. Unlike the wood samples, these samples collectively represent the properties of all the plastic components in the TLCB specimens, since they were sourced from a single sheet. The dimensions of the cut samples were approximately 24mm wide, 150mm long, and exactly 5.85mm thick. Two small roller supports were placed 100mm apart along the length of the samples. The samples were then loaded by a concentrated load from a UTM at the middle span with a rate of 1.3mm/min. until they ruptured. Similarly, the forces and flexural stress profiles with the displacements and strains were recorded. The proportional limit was found to be at an average of 56.95MPa, which theoretically cannot be reached by the plastic components of the TLCB specimens when they rupture.

The method to determine the MOE of both the wood and plastic components from ASTM D790 and ASTM D143 is similar. The necessary data were taken from the flexural tests and were used to solve for the MOE from the following function:

$$E = l^3 m / 4wd^3 \quad (3)$$

In which E is the Modulus of Elasticity, l is the beam span or distance between supports, d is the sample depth, w is the sample width, and m is the initial straight line gradient from the load and displacement graph.

Table 3. Component modulus of elasticity

Composite Beam Sample Designation	Wood Component Modulus of Elasticity E_w (Mpa)	Plastic Component Modulus of Elasticity E_p (Mpa)
Sample-1	4,669.24	2,133.93
Sample-2	8,128.68	
Sample-3	3,670.28	

In the test for the mechanical properties of the wood samples, the variations of their values were noted and summarized in Table 4.

Table 4. Precision of wood mechanical properties

Mechanical Property	Mean (MPa)	Standard Deviation (MPa)	Coefficient of Variation CV (%)
Flexural Comp. Yield Strength	28.72	11.32	39.415
Flexural Tensile Yield Strength	43.66	18.52	42.42
Flexural Ultimate Strength	47.13	18.17	38.55
Shear Strength	7.20	3.99	55.42
Modulus of Elasticity	5,489.40	2,339.62	42.62

These variations could be explained by the possible different sourcing of the planks from the trees or tree sections they were cut from, and the storage conditions before they were procured. The age of the tree and section influences the density and structure of earlywood and latewood in the planks. These parameters affect the density of the wood, thus having an impact on its mechanical properties.

As a reference, pine wood, being in the same family as the wood component, can have an early density of 250 $kg.m^{-3}$ to a late density of 700 $kg.m^{-3,}$ which corresponds to almost a four-times and 4.5-times difference in tensile strength and MOE, respectively, between the two stages [8]. Possible differences in the moisture levels of the wood planks likely also played a role in these variations. It was found that raising the moisture content of certain wood species from their typical range of 9%–14% to full saturation can reduce bending strength by approximately 39%–55% and lower MOE by nearly one-third. [9, 10].

Comparing the precision of the plastic and wood components' mechanical properties, the plastic component had precisions of 56.95 ± 0.90 MPa (CV = 1.58%) and 2,133.93 ± 9.34 MPa (CV = 0.44%) and the wood component had precisions of 28.72 ± 11.32 MPa (CV = 39.415%) and 5,489.40 ± 2,339.62 MPa (CV = 42.62%) on their proportional limit and MOE respectively. It is observed that the plastic material was vastly more consistent than the wood, as seen in the differences in their Coefficient of Variation (CV). This comparison and the uniqueness of wood justified the wood planks to be treated individually in terms of their mechanical properties, even when they were of the same species, as opposed to the plastic samples being treated collectively, since they were easily verified to originate from a single source.

2.5. Theoretical Analysis

2.5.1. Elastic and Plastic Beam Theories

The calculations for the theoretical flexural strengths and deformations of the TLCB specimens at the elastic and elasto-plastic or post elastic bending stages revolved around the application of the Transformed Section Method (TSM) to account for the influence of the differences in material properties within the TLCB assemblies and simplify the complexities therein.

The method transforms the composite section into a fictitious homogeneous material that can be analyzed in a traditional manner. This is accomplished by imposing a strain compatibility condition within the material components making up the cross-section by adjusting the geometry of each component by a ratio of its elastic modulus to the base material modulus, also known as the modular ratio [11].

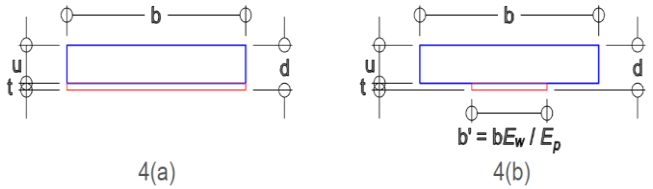

Fig. 4(a) Original cross-section, and (b) Transformed cross-section.

When the transformed or original cross-section of the multi-layered beam is subjected to an external moment, the internal stresses are in equilibrium. However, the transformed and original material internal stresses differ by a factor of their modulus ratio, with their strains being unaffected [12]. In the analyses, the top layer wood component served as the base material, and the width of the bottom layer plastic component is adjusted as shown in Figure 4.

The theoretical stress and strain profiles during bending were then determined at the yielding and rupture conditions of the TLCBs. The profiles reflected the applicable elastic and plastic behavior prior to and after the yielding of the components. The flexural strengths were calculated from the internal moments produced by the stress blocks.

Initially, the response of any material to bending is elastic, where its extreme fibers do not exceed their yielding stress and strain capacity. Increasing the bending load beyond the yielding moment will induce plastic behavior or start plastification in the material. To respond to the additional bending load, the stress in the fibers will propagate from the extremes towards the neutral axis while not exceeding the yielding values.

However, the strain in the fibers will continue to increase even after the yielding limit is reached. Thus, for any curvature past the yielding stage, its cross-section can be divided into elastic and plastic zones. Within the above or below the neutral axis, the section is elastic or termed the elastic core. Outside this zone, the strains exceed the yielding strain, and the material is plastified. As curvature increases, the elastic core progressively shrinks and plastification progressively spreads over the entire cross-section [13].

The middle span deflections of the TLCB specimens considered them to be simply supported at a 1400mm span with a concentrated load at their center. The maximum elastic deflection, or yielding deflection, occurs when one of the components yields.

The elastic deflections are calculated through the well-known Euler-Bernoulli beam theory. Given the strain profile and assuming small deformations, the yielding beam deflection is expressed as:

$$\delta_x = \int(\int \phi \, dx)dx \tag{4}$$

&

$$\phi = (\epsilon \leq \epsilon_y)/y \tag{5}$$

Where δ_x is the elastic deflection of the beam along its length, ϕ is the beam curvature, $(\epsilon \leq \epsilon_y)$ is the strain at the extreme fibre of the beam at or before yielding, and y is the distance of the extreme fiber to the neutral axis.

In the analysis for the elasto-plastic (post-yield condition) deformations of the TLCB specimens, the assumptions for simple plastic analysis were made [13]:

- Plasticity along the beams occurs exclusively at plastic hinges modeled as rigid-perfectly plastic hinges of zero length.
- Small-deformation theory is applicable, and geometric nonlinearity is not considered.
- The effect of strain-hardening is neglected.
- The TLCB specimens are properly braced to prevent instability.
- Plastic hinges can undergo an infinite amount of plastic deformation.
- Loads of constant relative magnitude are progressively increased without load reversal.
- Plane sections remain plane after bending.

Recognizing these assumptions past yielding, the elasto-plastic curvature is equal to a fictitious curvature where the beam had not yielded and maintained its full rigidity given the same strain conditions [14].

$$\phi = \frac{M_{ep}}{EI_{ep}} = \frac{M_1}{EI} \tag{6}$$

Where the beam curvature, ϕ, can be written in terms of the moment over the rigidity. M_{ep} is the elasto-plastic moment.

For a magnitude of its value, the beam's cross-section has a specific reduced flexural rigidity, EI_{ep}. M_1 is the fictitious moment that would exist if the beam did not yield and maintain its full rigidity, *EI*.

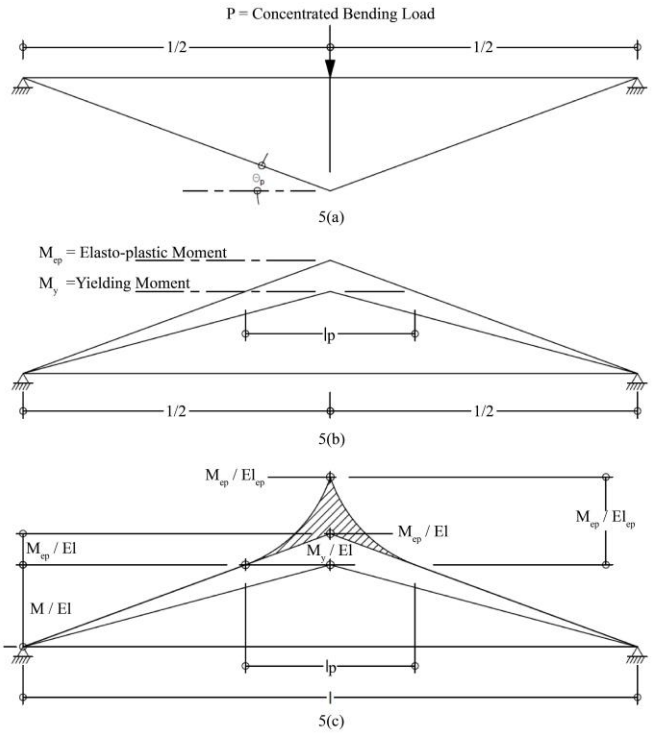

Fig. 5(a) Collapse mechanism, (b) Moment diagram, and (c) Curvature diagram.

The shaded area in Figure 5(c) is the inelastic rotation that occurs in addition to the elastic rotation past the yielding stage. The rotation of the plastic hinge was determined by calculating the shaded area [15]. The additional displacement due to plastic behaviour is computed as:

$$\Delta_p = \Theta_p(l/2) \tag{7}$$

Where Θ_p is the plastic hinge rotation, Δ_p is the additional inelastic deformation, and *l* is the supported beam span.

2.5.2. Theoretical Full Composite Flexural Analysis

The results of the calculation for the theoretical elastic and elasto-plastic full composite flexural strength of the TLCB specimens are presented through their respective stress and strain profiles below. It was observed that their neutral axis was always found to be on the wood component, even when it shifted slightly towards the bottom or tension region of the cross-section when they theoretically experienced plastic behaviour.

The TLCB specimens theoretically yielded by the compression region of the wood component reaching its proportional limit, rather than any yielding behavior in the plastic layer. Past the elastic bending stage, the compression region of the wood component partially plasticizes while its tensile region starts yielding. Just before rupture, both the tensile and compression regions of the wood component have been partially plasticized; at the same time, the plastic

component never reached its yield capacity. The full composite theoretical flexural ultimate strengths were calculated to average 1.89 times greater than their yield strengths with variations of 1.20 ± 0.42 Kn-m (CV = 35.00%) at yield and 2.22 ± 0.58 Kn-m (CV = 26.13%) at rupture.

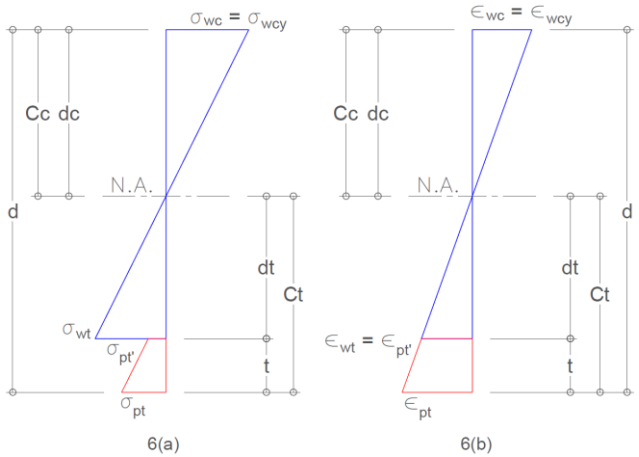

Fig. 6(a) Theoretical full composite elastic stress profile, and (b) Theoretical full composite elastic strain profile.

Table 5. Theoretical full composite elastic stress and strains

Composite Beam Sample Desig.	**Theoretical Elastic Moment at Yield M_y, (Kn-m)**	**Depth of Comp. Region Cc, (mm)**	**Depth of Tensile Region Ct, (mm)**
Sample-1	0.99	18.14	21.08
Sample-2	1.68	17.60	21.72
Sample-3	0.92	18.20	20.42
Composite Beam Sample Desig.	Depth of Elastic Comp. Wood Region from N.A. dc, (mm)	Depth of Elastic Tensile Wood Region from N.A. dt, (mm)	Stress at Extreme Comp. Wood Fiber s_{wc}, (MPa)
Sample-1	18.14	15.23	23.08
Sample-2	17.60	15.87	41.76
Sample-3	18.20	14.57	21.33
Composite Beam Sample Desig.	Stress at Extreme Tensile Wood Fiber s_{wt}, (MPa)	Tensile Plastic Fiber Stress at Wood-Plastic Interface $s_{pt'}$, (MPa)	Stress at Extreme Tensile Plastic Fiber s_{pt}, (MPa)
Sample-1	19.38	8.86	12.26
Sample-2	37.66	9.89	13.53
Sample-3	17.08	9.93	13.91
Composite Beam Sample Desig.	Strain at Extreme Comp. Wood Fiber v_{wc}, (%)	Strain at Extreme Tensile Wood Fiber and Wood-Plastic Interface v_{wt} & v_{pt}', (%)	Strain at Extreme Tensile Plastic Fiber v_{pt}, (%)
Sample-1	0.494344	0.415062	0.574488
Sample-2	0.513709	0.463353	0.634127
Sample-3	0.581195	0.465233	0.652038

Table 6. Theoretical full composite elasto-plastic stress and strains

Composite Beam Sample Desig.	Theoretical Elasto-plastic (Rupture) Moment M_{ep}, (Kn-m)	Depth of Comp. Region Cc, (mm)	Depth of Tensile Region Ct, (mm)
Sample-1	1.98	22.42	16.80
Sample-2	2.98	20.10	19.22
Sample-3	1.80	22.16	16.46
Composite Beam Sample Desig.	Depth of Elastic Comp. Wood Region from N.A. dc, (mm)	Depth of Elastic Tensile Wood Region from N.A. dt, (mm)	Depth of Plastic Comp. Wood Region pc, (mm)
Sample-1	4.27	6.40	18.14
Sample-2	6.45	10.04	13.65
Sample-3	4.90	7.24	17.26
Composite Beam Sample Desig.	Depth of Plastic Tensile Wood Region pt, (mm)	Tensile Plastic Fiber Stress at Wood-Plastic Interface $s_{pt'}$, (MPa)	Stress at Extreme Tensile Plastic Fiber s_{pt}, (MPa)
Sample-1	4.56	27.03	41.46
Sample-2	3.33	22.72	32.66
Sample-3	3.37	26.84	41.64

Composite Beam Sample Desig.	Strain at Extreme Compressive Wood Fiber v_{wc}, (%)	Strain at Ext. Tensile Wood Fiber & Wood-plastic Interface v_{wt} & $v_{pt'}$, (%)	Strain at Extreme Tensile Plastic Fiber v_{pt}, (%)
Sample-1	2.59253	1.26653	1.94305
Sample-2	1.60021	1.06456	1.94305
Sample-3	2.62685	1.25771	1.95117

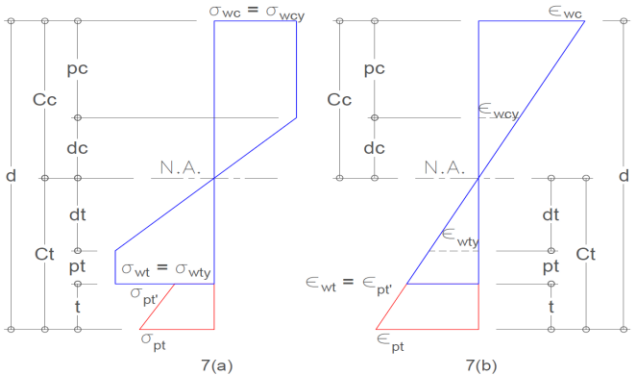

Fig. 7(a) Theoretical full composite elasto-plastic stress profile, And (b) Theoretical full composite elasto-plastic strain profile.

The middle span's elastic and plastic deformations were computed using the theories previously discussed and were supported by the resulting stress and strain profiles shown above. On average, the rupturing elasto-plastic deformations were 2.47 times the yielding elastic deflections, with variations of 48.12 ± 3.84 mm (CV = 7.98%) at yield and 118.75 ± 16.21 mm (CV = 13.65%) at rupture.

Table 7. Theoretical full composite deformations

Composite Beam Sample Designation	**Theoretical Full Composite Elastic Deformation at Yielding Δ_{Ce}, (mm)**	**Theoretical Full Composite Elasto-plastic Deformation at Rupture Δ_{Cep}, (mm)**
Sample-1	44.51	123.31
Sample-2	47.68	100.75
Sample-3	52.16	132.19

These variations were expected since the mechanical properties of the components and the total cross-sectional dimensions of the TLCB specimens also varied. However, they do not affect the specimens' flexural performance because the effectiveness and efficiencies only measure how much the baselines of theoretical flexural strengths and deformations are actually realized, rather than the raw magnitudes that have been achieved. This principle extended to the variations that existed in the theoretical non-composite flexural analysis.

2.5.3. Theoretical Non-Composite Flexural Analysis

The stress and strain profiles and flexural strengths of the theoretical non-composite assemblies were not necessarily required for the computations of their effectiveness, but were fundamental in calculating their deformations that were required to determine their efficiencies. The methods used in these calculations were similar to the theoretical full composite flexural analysis, but considered non-composite beam behavior.

The stress and strain profiles showed that two neutral axes existed at the cross-section, one for each of the wood and plastic components, initially located at half their respective depths. Throughout their bending, the neutral axis of the plastic component never moved, unlike the wood component, which shifted towards the tension region when plastic behavior was introduced.

Table 8. Theoretical non-composite elastic stress and strains

Composite Beam Sample Desig.	**Theoretical Elastic Moment M_y, (Kn-m)**	**Depth of Elastic Comp. Wood Region from N.A. dc, (mm)**	**Depth of Elastic Tensile Wood Region from N.A. dt, (mm)**
Sample-1	0.82	16.69	16.69
Sample-2	1.50	16.74	16.74
Sample-3	0.73	16.39	16.39
Composite Beam Sample Desig.	Stress at Extreme Compressive Wood Fiber s_{wc} (MPa)	Stress at Extreme Tensile Wood Fiber s_{wt}, (MPa)	Stress at Extreme Comp. Plastic Fiber s_{pc}, (MPa)
Sample-1	23.08	23.08	1.85
Sample-2	41.76	41.76	1.92
Sample-3	21.33	21.33	2.21
Composite Beam Sample Desig.	Stress at Extreme Tensile Plastic Fiber s_{pt}, (MPa)	Strain at Extreme Compressive Wood Fiber v_{wc}, (%)	Strain at Extreme Tensile Wood Fiber v_{wt}, (%)
Sample-1	1.85	0.494344	0.494344

Sample-2	1.92	0.513709	0.513709
Sample-3	2.21	0.581195	0.581195

Composite Beam Sample Desig.	Strain at Extreme Compressive Plastic Fiber v_{pc}, (%)	Strain at Extreme Tensile Plastic Fiber v_{pt}, (%)
Sample-1	0.086662	0.086662
Sample-2	0.089788	0.089788
Sample-3	0.103753	0.103753

Table 9. Theoretical non-composite elasto-plastic stress and strains

Composite Beam Sample Desig.	**Theoretical Elasto-plastic (Rupture) Moment M_{ep}, (Kn-m)**	**Depth of Elastic Comp. Wood Region from N.A. dc, (mm)**	**Depth of Elastic Tensile Wood Region from N.A. dt, (mm)**
Sample-1	1.38	5.78	8.64
Sample-2	2.44	7.30	11.36
Sample-3	1.19	6.87	10.14

Composite Beam Sample Desig.	Depth of Plastic Comp. Wood Region pc, (mm)	Stress at Extreme Comp. Wood Fiber s_{wc}, (MPa)	Depth of Plastic Tensile Wood Region pt, (mm)
Sample-1	12.79	23.08	6.16
Sample-2	11.05	41.76	3.77
Sample-3	11.03	21.33	4.73

Composite Beam Sample Desig.	Stress at Extreme Compression Plastic Fiber s_{pc}, (MPa)	Stress at Extreme Tensile Wood Fiber s_{wt}, (MPa)	Stress at Extreme Tensile Plastic Fiber s_{pt}, (MPa)
Sample-1	5.34	34.54	5.34
Sample-2	4.39	64.97	4.39
Sample-3	5.28	31.48	5.28

Composite Beam Sample Desig.	Strain at Extreme Compressive Wood Fiber v_{wc}, (%)	Strain at Extreme Tensile Wood Fiber v_{wt}, (%)
Sample-1	1.58883	1.26653
Sample-2	1.29141	1.06456
Sample-3	1.51383	1.25771

Composite Beam Sample Desig.	Strain at Extreme Compressive Plastic Fiber v_{pc}, (%)	Strain at Extreme Tensile Plastic Fiber v_{pt}, (%)
Sample-1	0.25028	0.25028
Sample-2	0.20589	0.20589
Sample-3	0.24738	0.24738

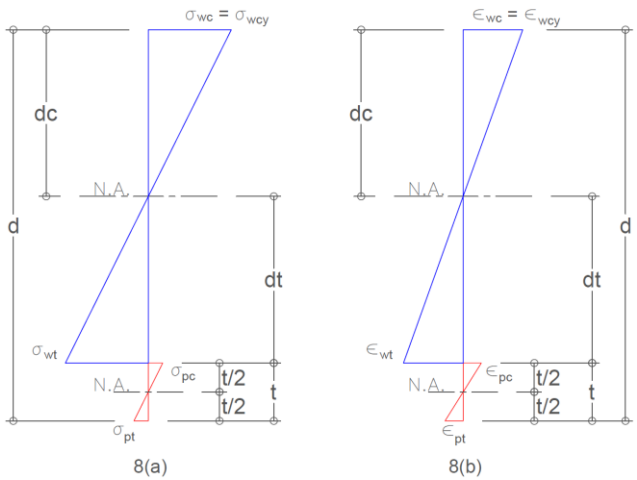

Fig. 8(a) Theoretical non-composite elastic stress profile, and (b) Theoretical non-composite elastic strain profile.

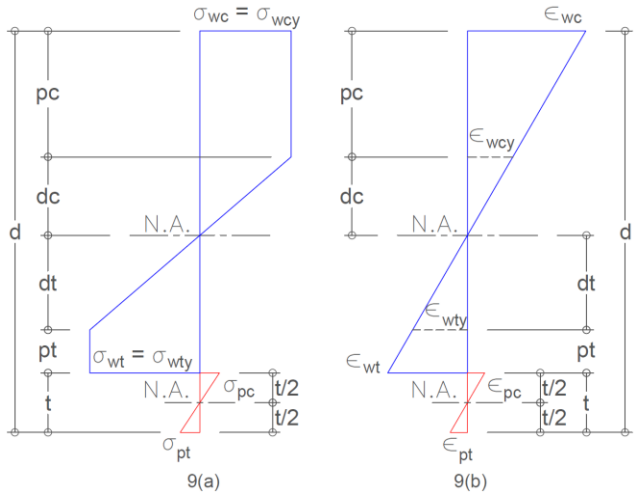

Fig. 9(a) Theoretical non-composite elasto-plastic stress profile, and (b) Theoretical non-composite elasto-plastic strain profile

The yielding and rupture sequence of the non-composite beams was the same as with the full composite behavior, and where, similarly, the plastic component never yielded.

The non-composite theoretical flexural ultimate strengths of the TLCB specimens were calculated to average 1.65 times greater than their yield strengths with variations of 1.02 ± 0.42

Kn-m (CV = 41.18%) at yield and 1.67 ± 0.67 Kn-m (CV = 40.12%) at rupture. When compared to their full composite counterparts, they were 0.83 and 0.73 times lower at yield and rupture, respectively.

On the other hand, the non-composite mid-span deformations at rupture were found to average 2.87 times greater than the elastic deflections with variations of 52.16 ± 5.08 mm (CV = 9.75%) at yield and 149.97 ± 23.90 mm (CV = 15.94 %) at rupture. The non-composite elastic and rupture deformations were observed to be greater than the full composite by an average of 1.08 at yield and 1.26 at rupture. Since the non-composites theoretically had greater deformations than the full composites while carrying lighter loads, the rigidity of the full composites being higher than their counterpart was confirmed.

Table 10. Theoretical non-composite deformations

Composite Beam Sample Designation	Theoretical Full Composite Elastic Deformation at Yielding Δ_{Ne}, (mm)	Theoretical Full Composite Elasto-plastic Deformation at Rupture Δ_{Nep} (mm)
Sample-1	48.39	153.26
Sample-2	50.14	124.59
Sample-3	57.94	172.05

2.5.4. Full Composite Behavior Shear Criteria

The TLCB specimens were intended to act as full composites throughout bending, with the interlocking grooves joining the two components. To guarantee the behavior, the wood grooves had to exhibit an adequate degree of shear connection and resistance against traverse or horizontal shear. The calculations herein only served to check if the TLCB specimens would act as full composites until rupture.

TSM was employed to the well-known traverse shear equations in determining the out-of-plane shear stress distribution of the transformed sections from the following functions [12]:

$$\tau_T^k = \frac{VQ_T}{I_T b_T^k} \tag{8}$$

&

$$\tau^k = N_1^k \bar{X}^k \tau_T^k \tag{9}$$

Where the superscript *k* is an identifier for the component layer, $\boldsymbol{\tau_T^k}$ is the transformed shear stress, *V* is the vertical shear load, Q_T is the transformed moment of area, and I_T is the transformed moment of inertia, $\boldsymbol{b_T^k}$ is the transformed width of the layer, $\boldsymbol{\tau^k}$ is the shear stress, $\boldsymbol{N_1^k}$ is the modular ratio and $\boldsymbol{\bar{X}^k}$is an in-plane shear coupling term considering the effects of Poisson's ratio. The TSM equation for transverse shear calculations presented can be and was reduced to the conventional TSM by neglecting Poisson's ratios and in-plane shear coupling terms [12], implying that $\boldsymbol{\bar{X}^k}$ = 1.

The critical transverse shear stress of the TLCB cross-section was computed at the plastic–wood boundary where interface slip took place, and considering the rupturing condition at the mid-span.

It was determined that the horizontal shear capacity, or the shear capacity parallel to the grain of the wood component, was at least 2.15 times greater than the traverse shear developed from the rupturing load. Thus, the grooves were ensured that they will not shear before the assemblies break from pure flexure.

Table 11. Theoretical traverse shear capacity of wood grooves

Composite Beam Sample Desig.	Vertical Shear at Mid-span (Rupture) V, (Kn)	Horizontal Shear Stress at the Wood Grooves t_g (MPa)	Horizontal Shear Capacity of the Wood Component t_h, (MPa)
Sample-1	2.83	1.26	2.71
Sample-2	4.26	2.19	8.59
Sample-3	2.57	1.09	10.31

The adequacy check of the wooden grooves against transverse shear is not enough to guarantee full composite action. The TLCB specimens must also be confirmed to have a degree of shear connection greater than one. The equation to calculate the degree of shear connection was taken from Structural Eurocode EN 1994-1-1:2004 [16].

$$\left(\mathrm{n} = \frac{n}{n_f}\right) > 1 \tag{10}$$

Where n is the degree of shear connection, *n* is the collective capacity of the shear connectors against interface slip, and n_f is the developed normal force of the component to slip.

The collective resistance against interface slip developed by the shear connectors was calculated from the point of zero to maximum moment or from one end of the support to the mid-span of the TLCB beam specimens. The normal force splitting the assembly, on the other hand, arose from the flexural stress on the plastic component determined by the stress profile of the cross-section at rupture.

Table 12. Degree of shear connection of TLCB

Composite Beam Sample Desig.	Collective Capacity of Shear Connectors against Interface Slip *n*, (Kn)	Developed Slipping Normal Force at Rupture n_f, (Kn)	Degree of Shear Connection, n
Sample-1	92.09	38.26	2.41
Sample-2	291.16	31.10	9.36
Sample-3	351.68	38.26	9.19

The minimum degree of shear connection among all the TLCB specimens was found to be 2.41, which theoretically guaranteed that no interface slip would occur throughout their bending.

Literature Review

3.1. TGI and Traditional Japanese Woodworking Techniques

Most present studies involving TGI are mostly manifested in the examination of traditional Japanese wood working techniques. The desirability to examine them stems from their proven reliability, evidenced by existing classical Japanese wooden structures and from available detailed surviving records and schematics of the joineries. The interlocking characteristics of the joints offered by these methods had inspired this research to exclusively incorporate grooves in connecting the components of the TLCB specimens. Records of these joints not only provided diagrams on how they may be replicated, but they also presented test results to describe how they may fail and behave under load. Two particular Japanese wood joinery connections were of interest to the research: the stepped dovetailed splice (koshikake aritsugi) and the stepped goose splice (koshikake kamatsugi). These two joinery configurations served to splice two wood segments of groundsills; however, their similar function to beams suggested they may have similar flexural behavior. Tensile tests on the joints showed that the tensile failure mode can occur through the formation of longitudinal cracks along the wood grain, and a combination of bearing and shear failure modes can happen on the interfaces of the interlocks [17]. While the presented failure modes do not necessarily completely represent the TLCB specimens, they demonstrated that these possibilities could take place when the specimens do rupture. These possibilities prompted the computations for the adequacy against horizontal shear to be considered in the study.

Investigations on traditional Japanese wood working joineries presently commonly focus on the feasibility of reproducing them rather than their structural applications. It is found that traditionally replicating these methods would be difficult since trained labor and craftsmen with significant years of experience are required to execute them properly. Additionally, the decline of these traditional techniques has not helped them to be learned by the present construction and manufacturing industry. However, it is proven that technological advancements in design software and fabrication machines can aid in reinventing and reviving these methods [3]. One such advance is found in Computer Numerically Controlled technology (CNC). CNC machines make it easier for less experienced workers to cut the intricate geometries of the woodworking joints with precision. However, CNC machines still rely on the skill of their operators who use them. This implies that even with these technological advantages, errors in reproducing these woodworking joints can still exist. Moreover, the cuts that a CNC machine can perform depend on the number of axes it has, furthering its reliance on operator skill. These limitations provoke innovations towards the fabrication of the joineries without compromising their overall integrity and purpose [2]. In the same manner, this research was inspired by the ideas found in traditional Japanese wood working techniques and innovated upon due to the limitations of the tools available to realize them. Thus, resulting in the components of the TLCB specimens being interlocked by geometrically fit grooves which were shaped by common power tools such as a single-axis router and circular saws.

3.2. Composite Action in Layered Beams

The components of typical composite and layered beams in the construction industry are commonly joined by mechanical fasteners in the form of bolts, rivets, or nails. The major parameters affecting composite action within composites are the discontinuities between component layers, the slip moduli of their connectors, and the modulus of elasticity of their components. Thompson's finite element method can be used to account for these effects based on the principle of minimum potential energy. The formula assumes that the component layers share the same curvature. The first two terms in the equation account for the flexural and axial strain energies, and the last term is for the work due to beam loading. The energy losses due to interface slip are represented by the third term [5].

$$\pi_p = \sum_{i=1}^{nL} \int_0^l [\,(1/2)E_iI_i(d^2y/dx^2)^2]\,dx + \sum_{i=1}^{nL} \int_0^l [(1/2)E_iA_i(du_i/dx)^2]\,dx + \sum_{i=1}^{nL-1} \int_0^l (1/2)(k_in_i/s_i)[(u_{i+1} - u_i) - (1/2)(h_{i+1} + h_i)(dy/dx)]^2 dx - \int_0^l w(y)dx \quad (11)$$

Where n_i is the number of layers, E_i is the modulus of elasticity of layer i, K_i is the slip modulus between i and i + 1, n_i is the number of rows of connectors between layers i and i + 1, s_i is the spacing of connectors between layers i and i + 1, h_i is the depth of layer i, w is the beam loading, x is the length along the beam, y is the vertical displacement of the beam, l is the beam length and u_i is the displacement of layer i.

The differences in modulus of elasticity of the components affect the distribution of axial forces in the cross-section, wherein stiffer materials tend to induce more resistance. They can be accounted for by simply substituting their values in the equation. Gaps between layers disrupt the propagation of energy to the components, causing them to be lost in the system. To determine their effects on composite action, substituting a small length and low elasticity for the gaps can be implemented in the solution. The slip moduli pertains to the property of the connectors to resist interface slip defined by their configuration and inherent stiffness. The moduli is a stiffness parameter used in the finite-element model determined through stress versus deflection graphs resulting from a slip-test setup of the connectors [5]. The paper used simpler solutions to account for the parameters affecting composite action as opposed to the finite element model, in the spirit of it being introductory research. The effects from the differences in modulus of elasticity were accounted for through TSM, and interface slip was justified to be negligible by ensuring the degree of shear connection of the TLCB specimens was greater than one. However, the consequences of the possible gaps between layers were not measured since instruments were not available to verify them. Despite this, it was assumed that the specimens did not have gaps since, upon close ocular inspection, no discontinuities between layers were apparent.

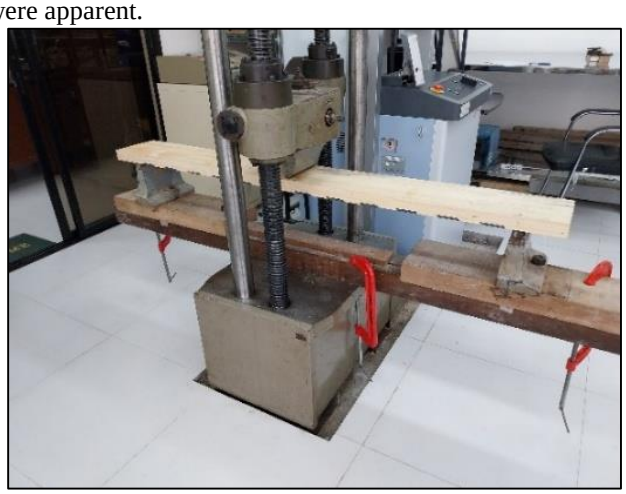

Fig. 10 TLCB specimen experimental set-up

Results and Discussion

4.1. Experimentation Summary

The three-point bending test procedure for the TLCB specimens was conducted through ASTM D198: Standard Test Methods for Static Tests of Lumber in Structural Sizes [18]. Each of the 1630mm long TLCB specimens was supported on its ends to create a 1400mm simply supported span. A load from a UTM was then pressed at their mid-span with a rate of 1.30mm/min until they ruptured. The loads and deformations the specimens experienced were recorded and presented in Figure 12. After rupture, their failure modes were observed and examined as shown in Figure 11.

4.2. Specimen Failure Modes

ASTM D198 provided six failure modes in which wood can rupture in bending, four ways by tension, one way by compression, and one way by traverse shear. Namely, these are simple tension, cross-grain tension, splintering tension, brash tension, compression, and horizontal shear. From this reference, it was observed that Samples 1 and 2 failed by cross-grain tension and Sample 3 failed by simple tension. It is of note that the longitudinal tensile cracks on the wood component were located to have started on the wood-plastic interface, and no signs of yield or rupture were seen on the plastic component for all specimens. This is evidence that the plastic component was able to transmit the flexural stress to the wood and also confirmed the theoretical yielding and rupture sequence of the TLCB specimens, where they would eventually rupture at the tensile region of the wood component without the plastic component even yielding.

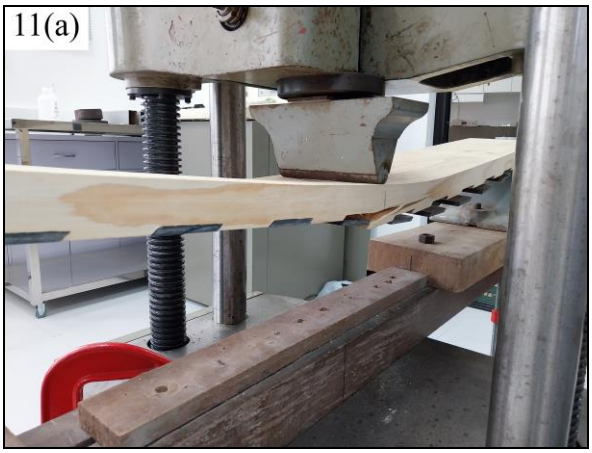

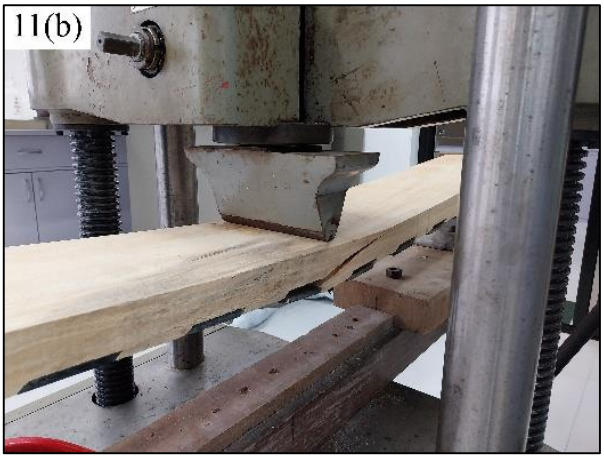

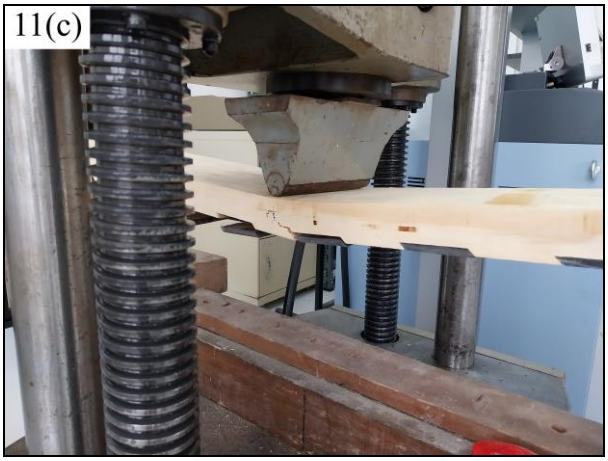

Fig. 11(a) Sample 1 failure mode, (b) Sample 2 failure mode, and (c) Sample 3 failure mode.

However, when the TLCB specimens were close to yielding, their components started to separate, but not completely. This occurrence was not captured in the theoretical calculations since they were intended and theoretically expected to act as full composites.

4.3. Effectiveness and Efficiencies

During the flexural tests of the TLCB specimen, their displacements and respective loads were recorded and compared with their theoretical values as summarized in Figure 12. The comparisons between theoretical and actual values through Equations 1 and 2 provided their effectiveness and efficiency. The calculations showed that the yielding flexural effectiveness of the TLCB specimens averaged at 66.98% with a standard deviation of 17.37% (CV = 25.94%) and was reduced to an average of 55.59% with a standard deviation of 10.12% (CV = 18.20%) at rupture.

Table 13. TLCB specimen flexural effectiveness

Composite Beam Sample Desig.	**Theoretical Full Composite Elastic Moment (Yielding) M_y, (Kn-m)**	**Actual Elastic Moment (Yielding) M_a, (Kn-m)**	**Elastic Flexural Effectiveness EFV, (%)**
Sample 1	0.99	0.86	87.04
Sample 2	1.68	0.95	56.65
Sample 3	0.92	0.52	57.25
Composite Beam Sample Desig.	Theoretical Full Composite Elasto-plastic Moment (Rupture) M_{ep}, (Kn-m)	Actual Elasto-plastic Moment (Rupture) M_a, (Kn-m)	Elasto-plastic Flexural Effectiveness EFV, (%)
Sample 1	1.98	1.29	65.04
Sample 2	2.98	1.69	56.81
Sample 3	1.80	0.81	44.92

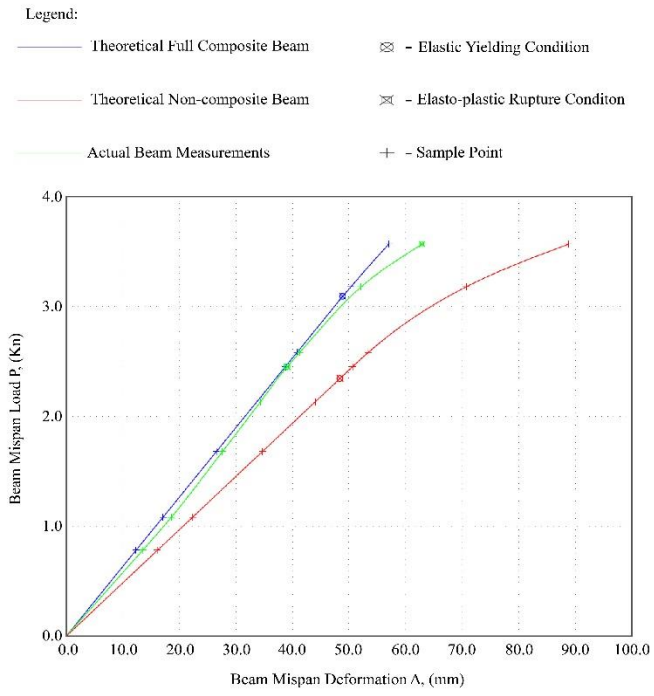

(a)

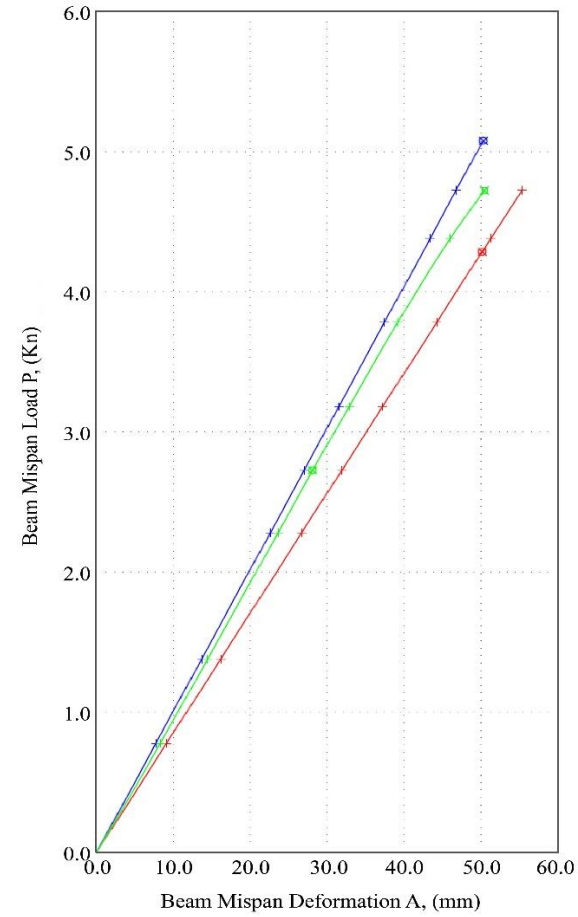

(b)

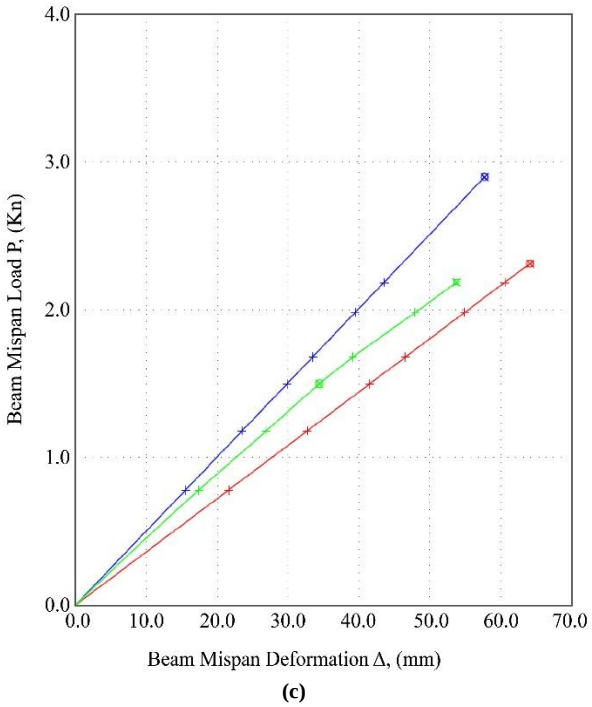

(c)

Fig. 12(a) Sample 1 load-displacement graph, (b) Sample 2 load-displacement graph, and (c) Sample 3 load-displacement graph.

It was found that the samples had greater average effectiveness at the yielding condition than at rupture by 11.39% and not once had they realized their elastic and elasto-plastic theoretical full composite flexural strength.

Additionally, their actual flexural strength was also less than their theoretical non-composite flexural strength by an average of 20.18 $\pm$ 22.06% at yield and 23.06 $\pm$ 14.34% at rupture, except for Sample 1, which exceeded its theoretical non-composite flexural strength at the yielding condition by 4.87%.

The flexural efficiencies were computed considering the deformations developed by the actual yielding and rupturing loads. It was observed that the flexural efficiencies of the composite beam assemblies were not constant. They were at 100% when unloaded and started to drop during loading. At some point during elastic bending, their efficiencies stopped decreasing and instead rose, peaking at the yielding condition, then continued to drop again until rupture.

Sample 3 was an exception whose efficiency dropped continuously from the start of loading until rupture. At the yielding condition, the average efficiency of the composite beam specimens was 78.53% with a standard deviation of 18.25% (CV = 23.24%). After yielding, the efficiencies of all beam samples continued to drop until rupture to an average of 59.55% with a standard deviation of 20.65% (CV = 34.68%).

The moderate to high variability observed in the effectiveness of the TLCB specimens was attributed to their high variability in efficiencies since the efficiency of a composite section does affect its effectiveness, as implied by their definitions discussed in the previous chapters. Further, this correlation is demonstrated by the differences in both of these properties between the highest and lowest ranges of the data set.

Sample 1 had the highest efficiencies of 97.28% and 81.18% at yield and rupture, with the highest effectiveness of 87.04% and 65.04% respectively. Comparatively, Sample 3 had the lowest efficiencies of 60.83% and 40.04% at yield and rupture, with the lowest corresponding effectiveness of 57.25% and 44.92%.

The high variability in the efficiencies could be explained by the randomness of the unintended observed separation of the plastic layer from the wood component during bending, which may have been exacerbated by the uniqueness of the wood material.

These variations highlight the effects of gaps between components in layered beams to composite action and the inability of the 45-degree grooves to completely retain full composite behavior within the specimens.

Table 14. TLCB specimen flexural efficiencies

Composite Beam Sample Desig.	**Actual Yielding Load P_y, (Kn)**	**Actual Yielding Moment M_y, (Kn-m)**	**Theoretical Full Composite Deflection Δ_C, (mm)**	**Actual Composite Deflection Δ_I, (mm)**	**Theoretical Non-Composite Deflection Δ_N, (mm)**	**Yielding Efficiency EFF, (%)**
Sample-1	2.45	0.86	38.74	39.07	50.62	97.28
Sample-2	2.73	0.95	27.01	28.12	31.91	77.49
Sample-3	1.50	0.52	29.86	34.43	41.52	60.83
Composite Beam Sample Desig.	Actual Rupture Load P_{ep}, (Kn)	Actual Rupture Moment M_{ep}, (Kn-m)	Theoretical Full Composite Deflection Δ_C, (mm)	Actual Composite Deflection Δ_I, (mm)	Theoretical Non-Composite Deflection Δ_N, (mm)	Rupture Efficiency EFF, (%)
Sample-1	3.57	1.25	57.00	62.99	88.81	81.18
Sample-2	4.72	1.65	46.77	50.42	55.35	57.43
Sample-3	2.18	0.76	43.55	53.75	60.56	40.04

5. Conclusion

All of the TLCB specimens were assembled with the intention of having them act as full composite beams or constantly be at 100% efficiency throughout their bending. However, the assemblies did not have constant efficiency or had the predicted full composite deflections. Most of them reached their maximum efficiency at yield, and all of them decreased in efficiency after yielding. The assemblies did not meet their expected performance at any point and are classified as partially composite, but it can be said that the beam specimens do have the most potential in being fully composite at the yielding condition. Additionally, the interlocking 45-grooves present in the assemblies were not sufficient in maintaining constant full composite action. The flexural strength of the assemblies was affected by composite action, proven by the theoretical full composite and non-composite calculations, wherein the former had greater strength than the latter. In hindsight, since the beam specimens were partial composites, they were expected to have lower flexural strengths than the theoretical full composite beams and have higher strengths than the theoretical non-composites, but only one of the three samples exhibited this at the yielding condition. By this evidence, the beam specimens are ineffective, although this may plausibly be attributed to the effects of partial composite action and the imperfections in the wood component rather than in the application of the concept of topological and geometric interlocking alone.

Due to the high variability and less-than-ideal results of the experiment, it was found that the viable application of TGI to structural layered beams is not optimistic, even when the flexural performance of the TLCB specimens at yield was consistently greater than at rupture. However, this may only be true if a 45-degree interlocking system is used alone. Other intricate configurations of TGI and materials may prove different results. It is encouraged that other TGI configurations be investigated with respect to the observations of the efficiencies and effectiveness of this paper.

Author's Contribution Statement

ER conceptualized, conducted the experiments, and analyzed the data for the research. DA and ER designed the study and wrote the manuscript. DA mentored ER in the study. All authors read and approved the manuscript.

Acknowledgements

The authors would like to thank God for granting His grace and giving them the strength to finish the research, the faculty of the College of Engineering and Architecture of the University of the Cordilleras for their support and guidance and the Department of Science and Technology – Forest Products Research and Development Institute (Philippines) for providing their technical expertise and instruments during the experiment and material testing phase of the study.

References

[1] Yuri Estrin, Vinayak R. Krishnamurthy, and Ergun Akleman, "Design of Architectured Materials based on Topological and Geometrical Interlocking," *Journal of Materials Research and Technology*, vol. 15, pp. 1165-1178, 2021. [CrossRef] [Google Scholar] [Publisher Link]

[2] Ahmed K. Ali, "Paradoxical Territories between Traditional and Digital Crafts in Japanese Joinery," *104th ACSA Annual Meeting Proceedings, Shaping New Knowledges*, pp. 342-347, 2016. [Google Scholar] [Publisher Link]

[3] David Yen, "*Japanese Timber Frame Methodology: Alternative Solutions to Hawaii's Built Environment*," D. Arch. Thesis, University of Hawai'i at Mānoa, 2012. [Google Scholar] [Publisher Link]

[4] R.M. Gutkowski et al., "Time-dependent Load Performance of Notched Wood-Concrete Composite Beams," *11th International*

Conference Structural Faults + Repair, University of Canterbury, pp. 13-15, 2006. [Google Scholar] [Publisher Link]

[5] J. Bodig et al., "*Tests and Analysis for Composite Action in Glulam Bridge Systems*," Colorado State University, Department of Civil Engineering, pp. 1-49, 1977. [Google Scholar] [Publisher Link]

[6] ASTM D143-22, "*Standard Test Methods for Clear Specimens of Timber*," ASTM International, 2022. [CrossRef] [Google Scholar] [Publisher Link]

[7] ASTM D790-17, "*Standard Test Methods for Flexural Properties of Unreinforced and Reinforced Plastics and Electrical Insulating Materials*," ASTM International, 2017. [CrossRef] [Google Scholar] [Publisher Link]

[8] Edward Roszyk, Waldemar Moliński, and Ewa Fabisiak, "Radial Variation of Mechanical Properties of Pine Wood (*Pinus Sylvestris* L.) Determined upon Tensile Stress," *Wood Research*, vol. 58, no. 3, pp. 329-342, 2013. [Google Scholar] [Publisher Link]

[9] Ágnes Vörös, Robert Németh, and Matyas Báder, "The Effect of Different Moisture Contents on Selected Mechanical Properties of Wood," *Gradus*, vol. 6, no. 3, pp. 75-81, 2019. [Google Scholar] [Publisher Link]

[10] Mohammed Kherais et al., "The Effect of Moisture Content on the Mechanical Properties of Wood Structure," *Pollack Periodica*, vol. 19, no. 1, pp. 41-46, 2024. [CrossRef] [Google Scholar] [Publisher Link]

[11] Wayne Hamilton, Stephen Tennyson, and Robert Hamilton, "Analysis by the Transformed-Section Method," *Proceedings of the 2001 American Society for Engineering Education Annual Conference and Exposition*, Albuquerque, New Mexico, pp. 1-11, 2001. [CrossRef] [Google Scholar] [Publisher Link]

[12] Aslam Kassimali, James N. Craddock, and Mehran Matinrad, "Bending and Traverse Shear Stresses in Fiber-Composite Beams by the Transformed-Section Method," *Composite Structures*, vol. 5, no. 1, pp. 33-49, 1986. [CrossRef] [Google Scholar] [Publisher Link]

[13] Michel Bruneau, Chia-Ming Uang, and Rafael Sabelli, *Ductile Design of Steel Structures*, 2nd ed., McGraw Hill, 2011. [Google Scholar] [Publisher Link]

[14] Barry T. Rosson, "Analysis of Inelastic Deformations," *122nd ASEE Annual Conference and Exposition*, Seattle, Washington, pp. 1-25, 2015. [CrossRef] [Google Scholar] [Publisher Link]

[15] Aldin Ali Kheyroddin, and Hosein Naderpour, "Plastic Hinge Rotation of Reinforced Concrete Beams," *International Journal of Civil Engineering*, vol. 5, no. 1, pp. 30-47, 2007. [Google Scholar]

[16] EN 1994-1-1, "*Eurocode 4: Design of Composite Steel and Concrete Structures-Part 1-1: General Rules and Rules for Buildings*," European Committee for Standardization, 2004. [Google Scholar] [Publisher Link]

[17] Torashichi Sumiyoshi, Gengo Matsui, and Ferenc Kovács, *Wood in Classical Japanese Architecture*, Kajima Institute Publishing, 1991. [Google Scholar]

[18] ASTM D198-22, "*Standard Test Methods of Static Tests of Lumber in Structural Sizes*," ASTM International, 2022. [CrossRef] [Google Scholar] [Publisher Link]